JACS
JOURNAL OF THE AMERICAN CHEMICAL SOCIETY
pubs.acs.org/JACS
Article

Variable Amine Spacing Determines Depolymerization Rate in Polydiketoenamines

Alexander R. Epstein, Jeremy Demarteau, Brett A. Helms,* and Kristin A. Persson*

Cite This: https://doi.org/10.1021/jacs.3c00772
Read Online

ABSTRACT: The design of circular polymers has emerged as a necessity due to the lack of efficient recycling methods for many commodity plastics, particularly those used in durable products. Among the promising circular polymers, polydiketoenamines (PDKs) stand out for their ability to undergo highly selective depolymerization in strong acid, allowing monomers to be recovered from additives and fillers. Varying the triketone monomer in PDK variants is known to strongly affect the depolymerization rate; however, it remains unclear how the chemistry of the cross-linker, far from the reaction center, affects the depolymerization rate. Notably, we found that a proximal amine in the cross-linker dramatically accelerates PDK depolymerization when compared to cross-linkers obviating this functionality. Moreover, the spacing between this amine and the diketoenamine bond offers a previously unexplored opportunity to tune PDK depolymerization rates. In this way, the molecular basis for PDK circularity is revealed and further suggests new targets for the amine monomer design to diversify PDK properties, while ensuring circularity in chemical recycling.

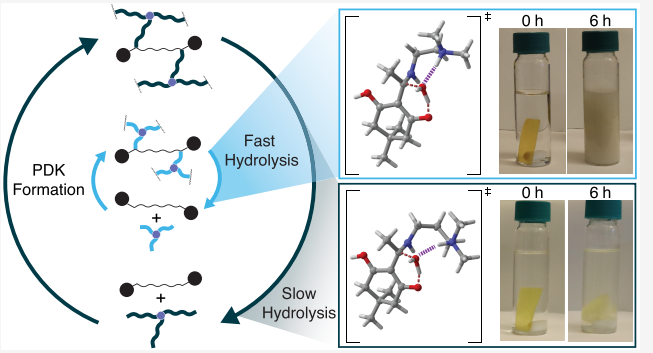

INTRODUCTION

Despite increasing attention paid to reducing plastic waste, plastics continue to accumulate in the environment and landfills, causing ecological harm and wasting nonrenewable resources.[1] Solving this problem is a multifaceted issue, but one critical strategy toward a future with minimal waste is fundamentally a materials challenge: can we synthesize circular plastics—plastics that can be infinitely recycled back to their constituent monomers—that are recycled through green processes and provide significant value to society? Recent discoveries in circular polymers have demonstrated rapid depolymerization under mild conditions, i.e., through acidolysis,[2−4] solvolysis,[5−8] or catalytic ring-closing,[9−13] showing a great potential to replace hard-to-recycle plastics. A new class of circular polymers, polydiketoenamines (PDKs), provides a promising step toward that goal. PDKs can be recycled back to monomers with high yield at room temperature in strong aqueous acid but remain stable in neutral, basic, and mildly acidic conditions.[2,14] This controlled recycling is enabled through the presence of the hydrolyzable diketoenamine moiety in the polymer repeat unit. As long as the diketoenamine moiety is maintained, the chemistry of PDKs can in theory be tailored to access specific properties while maintaining their recyclability. For example, heteroatom substitutions on the triketone monomer enable circularity in mixed-plastic recycling by differentiating the hydrolysis rate of the diketoenamine.[15] However, to access a wide range of properties, it is often necessary to alter the chemistry of the cross-linker. To further expand the scope of properties that PDKs can access while maintaining circularity in chemical recycling, we must therefore understand how the cross-linker affects the kinetics of the hydrolysis reaction.

Here, we vary the amine spacing, i.e., the carbon spacing between the secondary and tertiary amine in a triamine cross-linker, to understand the role that the tertiary amine plays in the hydrolysis reaction (Figure 1). We combine computational modeling and experiment to gain mechanistic insight into the role of amine spacing in diketoenamine hydrolysis and how that translates to PDK depolymerization. This combined approach also allows us to demonstrate that it is critical to use multipath transition state theory (MP-TST) to accurately connect simulations of diketoenamines with experiments, due to the large conformational freedom and strong noncovalent bonds in diketoenamines. Multipath formulations of transition state theory have previously been shown to yield highly accurate rate constants for hydrogen shift reactions,[16,17] especially when coupled with calculations of proton tunneling rates, and OH reactions.[18] Here, we demonstrate that MP-TST based on an ensemble of low-energy conformers yields highly accurate rate

Received: January 19, 2023

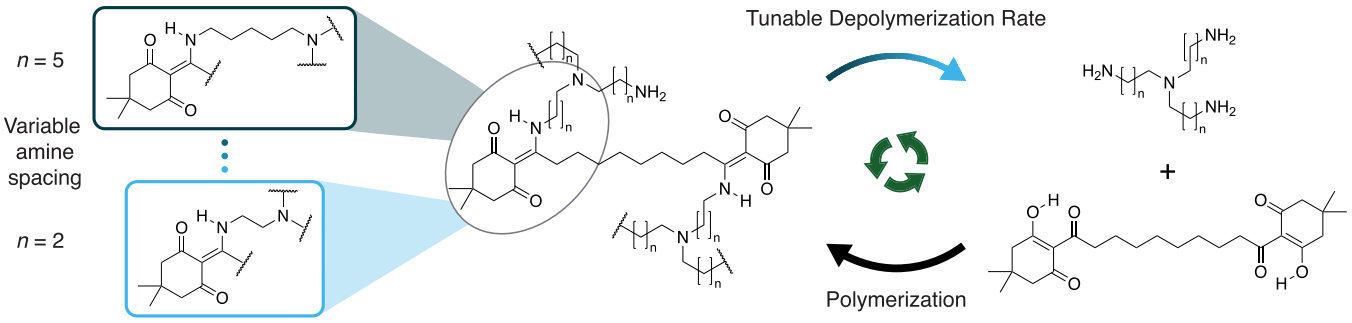

Figure 1. Varying the amine spacing in circular polydiketoenamines tunes their depolymerization rate.

constants for diketoenamine hydrolysis when compared to experiment. Furthermore, analyzing the pathways that contribute to the reaction, we find that the observed differences in the reaction rates are due to a highly variable stabilization of the transition state, which depends on an intramolecular hydrogen bond that forms during the addition of water. We find that a cross-linker heteroatom that is capable of forming a hydrogen bond while simultaneously minimizing strain energy is essential for low-energy depolymerization of PDK resins. Indeed, we highlight that stabilization due to intramolecular hydrogen bonds in a transition state can drastically change the rate of a reaction.

The findings presented here guide future work on PDKs to consider how remote substituents will influence depolymerization kinetics, even when the chemistry of the reaction center is not directly altered. With this in mind, we can design PDKs to access diverse properties while maintaining recyclability through low-temperature hydrolysis.

RESULTS AND DISCUSSION

We first discuss hydrolysis rates of diketoenamines with varying amine spacing and compare those results to measurements of hydrolysis kinetics of as-synthesized diketoenamines. We then analyze the calculated reaction pathways to understand the chemical origins of the observed differences in rate constant and investigate the advantages of using the MP-TST formalism for achieving high accuracy in comparison to experiment. Finally, we synthesize two PDK materials with varying amine spacing to verify that the small-molecule study translates to polymer systems.

Diketoenamine Hydrolysis Rate. Five variations of the diketoenamine (DKE) chemistry were examined: DKE **1**, which serves as the control with no tertiary amine, and DKEs **2**, **3**, **4**, and **5**, which have increasing carbon spacing from 2 to 5 carbons between the two nitrogen atoms (Figure 2a). To calculate the hydrolysis rate constant, we focused on the addition of water in the two-step addition−elimination hydrolysis reaction, as previous mechanistic studies of DKE **1** hydrolysis show the addition of H_2O to be rate-limiting.[15] We found that the MP-TST-calculated hydrolysis rate constant for DKE **2** is 113 times larger than the control, DKE **1**. The rate then dramatically decreases for DKE **3**, to just 6 times greater than DKE **1**, and then continues to decrease until DKE **5** shows no increase in rate compared to DKE **1** (Table 1). The experimentally observed rate constants closely follow this trend (Figure 2b). These observed rate constants were determined via ^{1}H NMR kinetics at different temperatures (Figures S1−S5). The only significant discrepancy between simulations and experimental observations is the relative rate constant of DKE **5**. Experimentally, DKE **5** hydrolyzes slightly faster than DKE **1**, at $k_{relative}$ = 1.5, whereas the calculations predict that DKE **5** hydrolyzes slower than DKE **1**, at $k_{relative}$ = 0.76. While this result for DKE **5** leads to a qualitative error in the trend, the absolute difference is small and still indicates that the molecules hydrolyze at similar rates. In addition, we report values for the methods that we consider to be the best available for a system of this size, but the quantitative rate constant calculation is sensitive to the method of approximating the vibrational entropy and the hybrid-DFT level of theory (Tables S1 and S2). Regardless, these data show a substantial difference in the hydrolysis rate for structures that only differ by substitutions far from the reaction center.

Table 1. MP-TST Calculated and Experimental Relative Rate Constants of Diketoenamine Hydrolysis

molecule	calculated $k_{relative}$	observed $k_{relative}$
DKE **1**	1.0	1.0
DKE **2**	112.7	178.9
DKE **3**	6.3	10.4
DKE **4**	2.1	2.6
DKE **5**	0.76	1.4

To further understand the rapid decrease in reaction rate with amine spacing, we analyzed the dominant reaction pathways contributing to the calculated MP-TST rate for each DKE. All DKEs with tertiary amines display similar, critical features in the reactant and transition state. First, the most stable states of the reactant exhibit a planar conformation due to a six-membered hydrogen-bonded ring bearing the exchangeable proton and a slightly nonplanar conformation with both amines coordinating to the ketone. During the addition of water, the hydrogen bonds break to reach a tetrahedral intermediate where the tertiary amine coordinates with the incoming water to lower the energy of the transition state.

The variation in reaction rate can be qualitatively understood by analyzing the energetics of the single dominant pathway for each DKE. In all cases, the free energy barrier has significant enthalpic and entropic components at room temperature. However, the entropic contribution is similar for all 5 DKEs and does not trend with the overall free energy barrier, while the enthalpic contributions differ significantly and mirror the trend in the overall barrier (Table S3). Further analyzing the enthalpy barrier, we see that the variation in hydrolysis rate arises from an energetic balance in the transition state between the stabilization due to the formation of an intramolecular hydrogen bond and the strain due to reaching that conformation. This trend can be quantified by examining the distortion and interaction contributions to the energy barrier:[19]

$$\Delta E^{\ddagger}_{\text{Total}} = \Delta E^{\ddagger}_{\text{Interaction}} + \Delta E^{\ddagger}_{\text{Distortion}} \quad (1)$$

https://doi.org/10.1021/jacs.3c00772
J. Am. Chem. Soc. XXXX, XXX, XXX−XXX

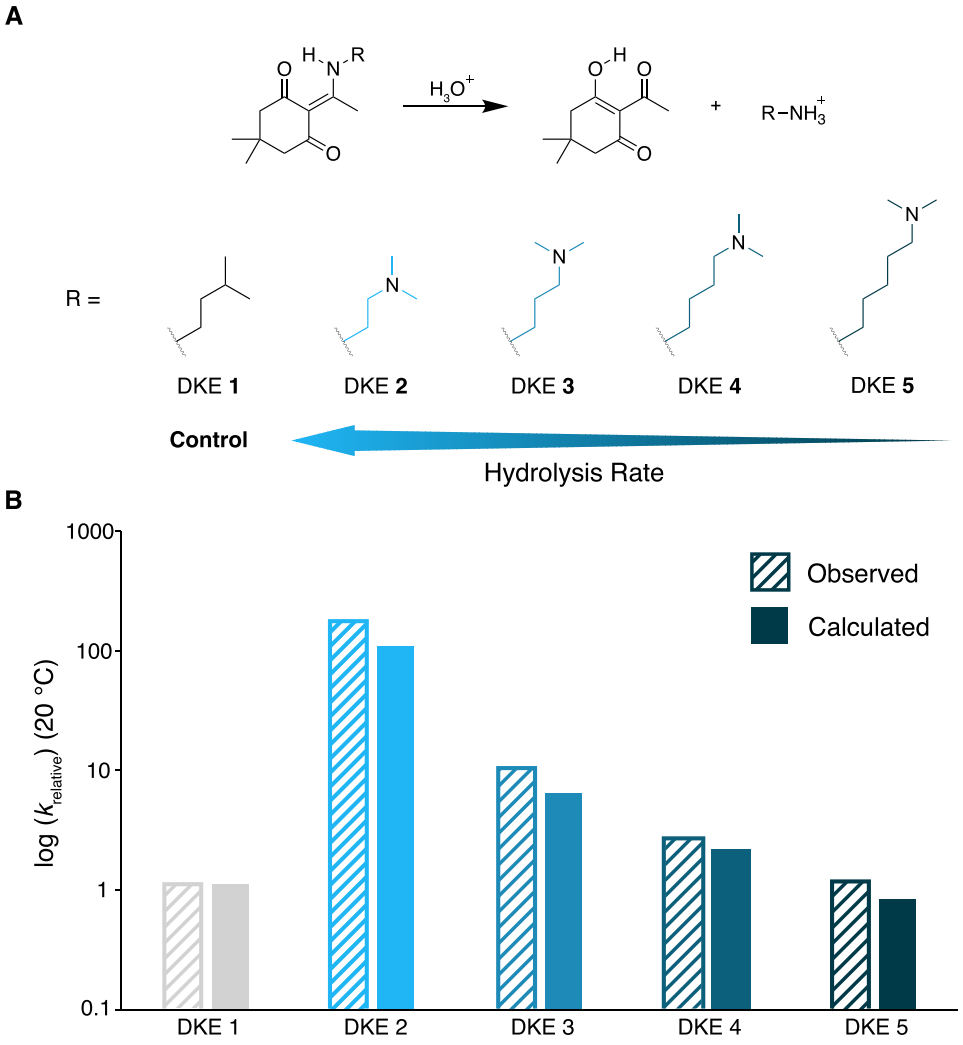

Figure 2. Variation of the diketoenamine hydrolysis rate with increasing amine spacing. (a) Structures of DKE **1**, the control, and DKEs **2**−**5**, with increasing amine spacing. (b) Calculated (MP-TST) and observed reaction rates for DKEs **1**−**5** show excellent agreement and a dramatic decrease in reaction rate with increasing amine spacing.

This energy decomposition separates $\Delta E^{\ddagger}_{\text{Interaction}}$, the change in energy due to the mixing of electronic states in the two molecules, from $\Delta E^{\ddagger}_{\text{Distortion}}$, the change in energy due to straining the geometries of each molecule individually. Analyzing the dominant mechanism for each DKE, we observe a monotonic trend in the energy barrier that is consistent with the observed trend in hydrolysis rate and is reproduced in $\Delta E^{\ddagger}_{\text{Total}}$ and $\Delta E^{\ddagger}_{\text{Distortion}}$ but not $\Delta E^{\ddagger}_{\text{Interaction}}$ (Figure 3). While larger amine spacings trend with increased stabilization of the transition state, the unfavorable distortion of a longer chain into the low-energy transition state ultimately dominates the energy barrier, leading to a steady increase in the kinetic barrier.

Origins of the MP-TST Rate. While an energy decomposition based on a single pathway is useful for understanding the mechanistic origins of the decrease in rate with increasing amine spacing, the high accuracy of the rate predictions in comparison to experiment shown in Figure 2 requires a method that takes into account the numerous reaction pathways available to this system. With two to five carbons between amines, there are up to seven rotatable bonds in a DKE, and the ketone, enol, iminium, tertiary amine, and water are all available to participate in hydrogen bonds. A standard approach to computational studies of the reaction rate for a bimolecular reaction with organic molecules of medium size and flexibility is to perform a conformer search of the transition state and calculate the energy barrier, $\Delta E^{\ddagger}$, as the difference in energy between the lowest-energy transition state and lowest-energy reactant, assuming facile interconversion among reactant conformers. Single-structure transition state theory (SS-TST) can then be used to obtain a reaction rate constant:

$$k_{\text{SS-TST}} = \kappa \frac{k_B T}{h} \frac{Q_{\text{TS}}}{Q_{\text{R}}} e^{-\Delta E^{\ddagger}/k_B T} \tag{2}$$

where $Q_{\text{TS,R}}$ are the partition functions of the transition state and reactants, k_B is the Boltzmann constant, h is the Planck constant, T is the temperature, and κ is the tunneling coefficient.

To accurately represent systems with large conformational freedom, MP-TST allows many-to-many relationships between reactant and product phase space.[16,20] Full MP-TST requires the identification of all distinct conformers of the transition state, and the SS-TST rate constant can be modified to be:

$$k_{\text{MP-TST}} = \frac{k_B T}{h} \frac{\sum_i^{\text{TS}_{\text{conf}}} \kappa_i e^{-\Delta E_i/k_B T} Q_{\text{TS},i}}{\sum_j^{\text{R}_{\text{conf}}} e^{-\Delta E_j/k_B T} Q_{\text{R},j}} e^{-(E_{\text{TS},0} - E_{\text{R},0})/k_B T} \tag{3}$$

https://doi.org/10.1021/jacs.3c00772
J. Am. Chem. Soc. XXXX, XXX, XXX−XXX

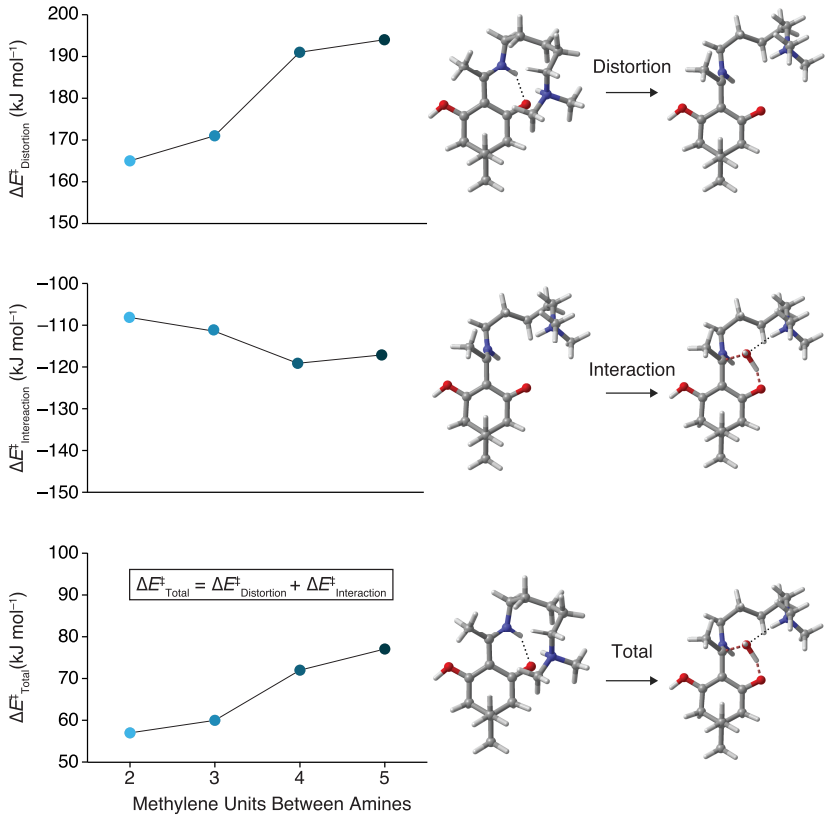

Figure 3. Decomposition of the energy barrier, $\Delta E^{\ddagger}_{Total}$, in the distortion−interaction model. The distortion energy $\Delta E^{\ddagger}_{Distortion}$ trends with the total energy barrier, while the interaction energy $\Delta E^{\ddagger}_{Interaction}$ does not.

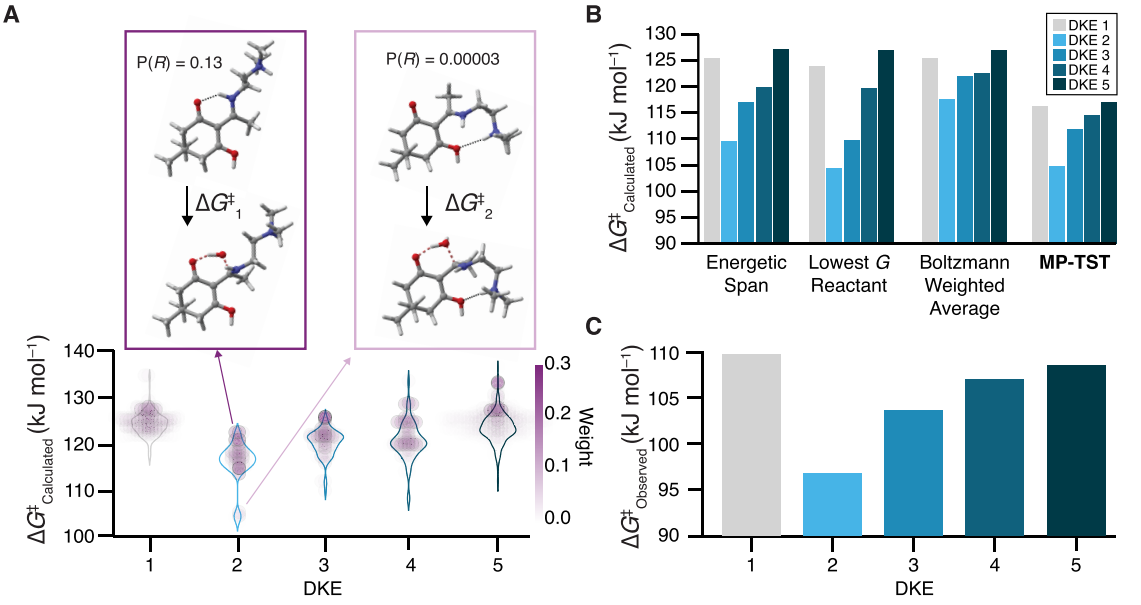

Figure 4. Calculated and observed hydrolysis free energy barriers. (a) Distribution of calculated free energy barriers contributing to the multipath transition state theory rate calculation. Points are shaded by the Boltzmann probability of the reactant for a given path. (b) Comparison of methods for extracting the hydrolysis free energy barrier from the distribution of reaction paths. (c) Free energy barriers calculated from an Eyring analysis of the observed rates.

Here, the single partition functions in eq 2 have been replaced by sums over all the partition functions of all conformers weighted by their relative energy to the lowest-energy conformer, and the energy barrier in the exponential term is the difference in the zero-point-corrected electronic energy between the lowest-energy transition state conformer, $E_{TS,0}$, and the lowest-energy reactant conformer, $E_{R,0}$. While MP-TST is formally true only for a sum over all conformers of the system, Møller et al. showed that accurate rate constants can be calculated by only including the low-lying conformers.[16] This

https://doi.org/10.1021/jacs.3c00772
J. Am. Chem. Soc. XXXX, XXX, XXX−XXX

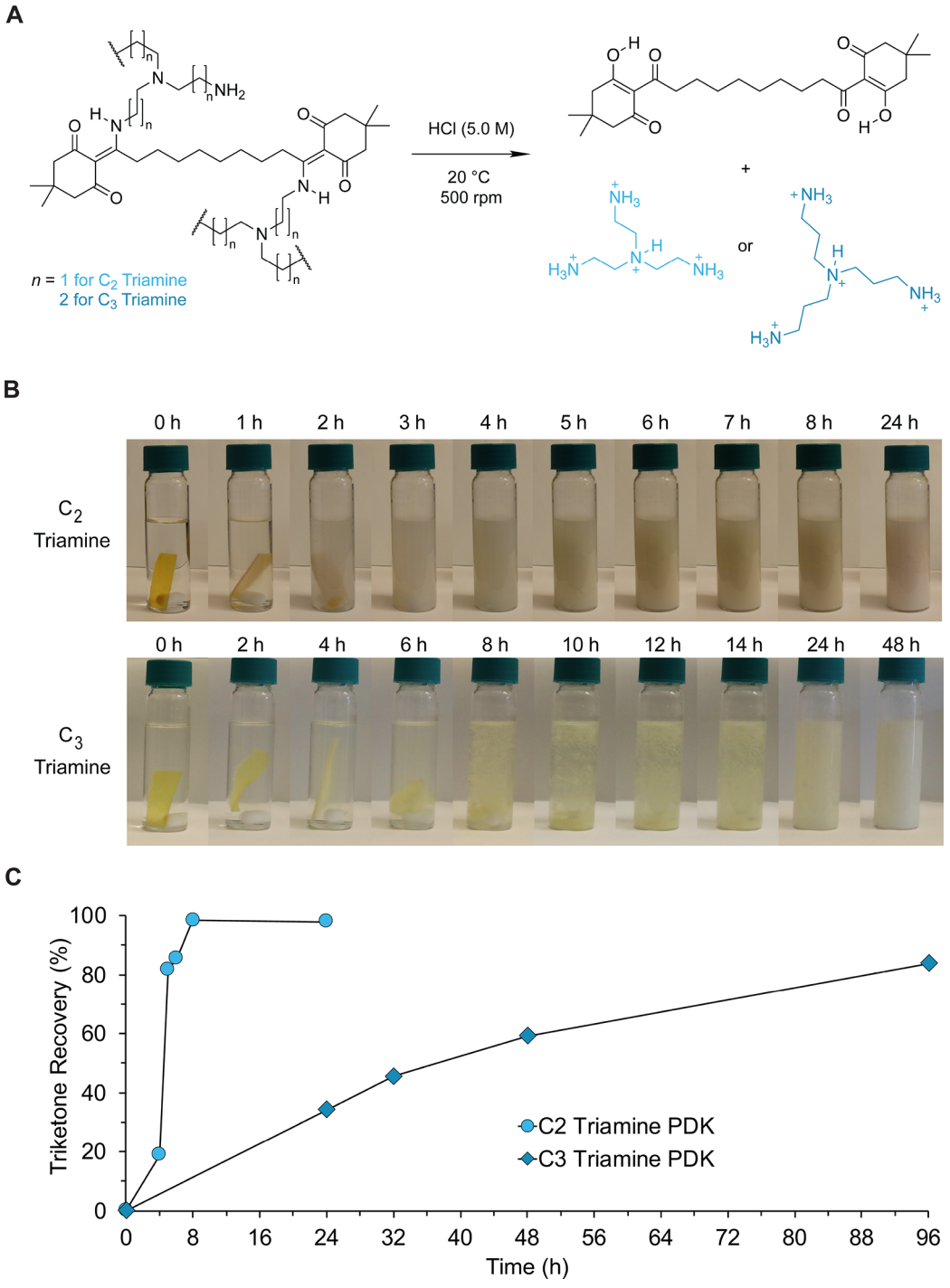

Figure 5. C_2 and C_3 PDK formulation hydrolysis. (a) Hydrolysis reaction pathway of PDKs into the corresponding triketone and C_2 and C_3 ammonium monomers. (b) Visual deconstruction of the PDK networks over time. (c) Kinetics of triketone recovery over time.

approximation is necessary when considering systems as large as those studied here, where calculating the partition function of every conformer at a high level of electronic structure theory is currently not computationally feasible.

The impact of a multipath model is perhaps best understood by examining the free energy barrier for the reaction. By analyzing the distribution of pathways, we find that all DKEs contain reaction coordinates with a range of free energy barriers, but that tertiary amine-containing DKEs exhibit specific conformations with significant contributions, whereas DKE **1** has a roughly equal contribution from many pathways (Figure 4a). Extracting one free energy barrier from that data is therefore not an obvious task. An energetic span approach,

$$\Delta G^{\ddagger} = G_{TS,0} - G_{R,0} \tag{4}$$

shows a close match with the trends in $\Delta G^{\ddagger}_{Observed}$ derived from an Eyring analysis of experimental rates (Figure 4b,c). However, the energetic span approach also overestimates the relative $\Delta G^{\ddagger}$ for DKE **5** compared to DKEs **2**–**4** and to a lesser extent the control, DKE **1**. As the choice of hybrid-DFT level of theory can systematically impact the absolute free energy barriers, we place more importance on the proper relative ordering of $\Delta G^{\ddagger}$.

https://doi.org/10.1021/jacs.3c00772
J. Am. Chem. Soc. XXXX, XXX, XXX−XXX

However, when comparing DKE **1** to DKE **5**, the observed difference in $\Delta G^{\ddagger}$ that we aim to capture, +1.1 kJ mol^{-1}, is within the accuracy of the ωB97X-V functional for hydrolysis barrier heights: a mean absolute error (MAE) of 2.89 kJ mol^{-1} when compared to highly accurate wave function methods.[21] Still, we would expect the relative $\Delta G^{\ddagger}$ of similar molecules to be more accurate than the MAE over a large data set, and the error in $\Delta\Delta G^{\ddagger}$ for DKE **1** and DKE **5** from the energetic span approach is 2.8 kJ mol^{-1}. Considering that errors are exponentiated when calculating the relative rate constant, higher accuracy is needed. Other reasonable approaches to calculating $\Delta G^{\ddagger}$ encounter similar discrepancies. For example, we can calculate the free energy barrier of the reaction coordinate connecting the lowest free energy reactant with its corresponding transition state:

$$\Delta G^{\ddagger} = G_{\mathrm{TS,R^*}} - G_{\mathrm{R^*}} \tag{5}$$

Or, we can use a Boltzmann-weighted average:

$$\Delta G^{\ddagger} = \sum_{j}^{\mathrm{R_{conf}}} \mathrm{e}^{-\Delta G_j/k_{\mathrm{B}}T}(G_{\mathrm{TS},j} - G_{\mathrm{R},j}) \tag{6}$$

where ΔG_j is the free energy difference between the lowest-energy reactant and the j^{th} reactant and $G_{\mathrm{TS},j}$ is the free energy of the transition state connected to the j^{th} reactant. Both of these methods underestimate the relative barrier for DKE **1** compared to the tertiary-amine-containing DKEs. In addition, both methods improperly space DKEs **2**−**4**. The lowest free energy reactant method results in a large gap between DKE **3** and DKE **4**, rather than between DKE **2** and DKE **3**, and the Boltzmann-weighted average gives almost identical barriers for DKE **3** and DKE **4**.

Instead, we obtain $\Delta G^{\ddagger}$ from the MP-TST rate:

$$\Delta G^{\ddagger} = \ln\left(k_{\mathrm{MP\text{-}TST}}\frac{h}{k_{\mathrm{B}}T}\right)RT \tag{7}$$

and find excellent agreement with the trends in experimental free energy barriers. MP-TST reveals all the critical features in the experimental trend in hydrolysis rate constants: the sharp increase in barrier from DKE **2** to DKE **3**, the plateau to DKE **5**, and the similar barrier for DKE **1** and DKE **5**. This agreement emphasizes the utility of a multipath approach for calculating reaction rates in systems with a large number of reactant and transition state conformations, capturing the differences between systems that favor a few conformers and those with more flat conformer distributions.

Depolymerization of PDKs. To test our understanding and predictions of the calculated hydrolysis rates of DKE **2** and DKE **3** small molecules, we employ two triamine monomers varying only in amine spacing to experimentally study their recycling behavior at the macromolecular level. We prepared two PDK resins via polycondensation of either tris(2-aminoethyl)amine or tris(3-aminopropyl)amine with a ditopic triketone monomer. We then compression-molded these materials into solid-bar samples prior to immersing them in 5.0 M HCl at 20 °C to study their depolymerization over time (Figure 5a). The deconstruction of the PDK networks gives rise to a precipitate comprising the triketone monomer; the liberated ammonium cross-linker (either C_2 or C_3) remains soluble in acid (Figure 5b). The C_2 triamine PDK is faster to depolymerize compared to the C_3 triamine PDK: precipitation of the monomer starts at 2−3 h for C_2 triamine PDK, while the macroscopic cleavage of the solid C_3 triamine PDK into an intermediate swollen network appears at 8−10 h.

In order to anchor our visual interpretations of PDK acidolysis, we determine the kinetics of the reaction by mass recovery of the triketone monomer at different time points (Figure 5c). Each experimental data point corresponds to a single sample that is filtered, basified, and precipitated in acid to ensure only the triketone monomer is recovered, as previously reported.[15] The mass gravimetry difference between the starting and recovered materials allows us to determine the triketone recovery percentage shown in Figure 5c. The C_2 triamine PDK reaches a maximum of depolymerization after 8 h, and the C_3 triamine PDK takes about 96 h to reach 80% recovery. ^{1}H NMR spectra of the recovered monomer showed perfect overlap of the peaks with the spectra of the pristine triketone for both formulations (Figures S6 and S7). These macromolecular findings regarding the recycling rates confirm what has been observed at the small-molecule level, where DKE **2** hydrolyzes faster than DKE **3**.

EXPERIMENTAL SECTION

We used a multistage conformer search method to identify the contributions to the MP-TST rate calculation. First, a candidate transition state structure for the addition of water for each DKE was taken from the assumed hydrolysis reaction pathway (Figure S8). The transition state was identified by optimization to a saddle point geometry using Gaussian16 at the ωb97XD/6-311+G(d,p)/SMD level of theory.[22−24] We then performed an extensive conformer search using CREST to identify the ensemble of conformers with the lowest free energy (Figure 6).[25] Final transition state geometries were optimized at

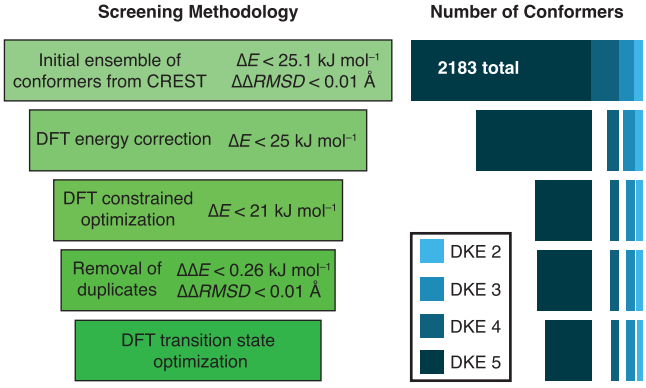

Figure 6. Procedure for identifying the lowest energy conformers of the addition transition state. A Δ refers to values calculated with respect to the lowest-energy structure and a ΔΔ refers to values comparing each structure to all others.

the ωb97XD/6-311+G(d,p)/SMD level of theory. Reactants were then generated by perturbing transition state structures along the vibrational mode corresponding to the single imaginary frequency in the Hessian to generate reactants. Reactants were then also optimized at the ωb97XD/6-311+G(d,p)/SMD level of theory. The free energy of the reactant was taken with the H_2O and DKE at infinite separation due to the variability in energies from small differences in the location of the single water molecule and the frequent failures in geometry optimization with one explicit water molecule. The final free energy includes a correction to the electronic energy with single-point calculations at the ωb97M-V/def2-TZVPD/SMD level of theory using Q-Chem 4.2.[26−28] Single-point corrections at ωb97XD/6-311++G(2df,2p)/SMD were also considered but overpredicted the acceleration of the hydrolysis in DKE **2**. The distortion−interaction energy decomposition was performed at the ωb97M-V/def2-TZVPPD/SMD level of theory. Gaussian16

https://doi.org/10.1021/jacs.3c00772
J. Am. Chem. Soc. XXXX, XXX, XXX−XXX

calculations were automated using QUACC,[29] and Q-Chem calculations were automated using Atomate.[30]

For the MP-TST calculations described in eq 3, partition functions were calculated in the quasi-rigid rotor harmonic oscillator approximation.[31]

Experimental methods and characterization of all molecules used in the studies are available in the SI.

CONCLUSIONS

In this work, we demonstrate how accurate simulations based on DFT calculations and MP-TST modeling can help design circular polymer formulations where the placement of the amine can strongly influence the rate of depolymerization. The presence of a tertiary amine in proximity to the hydrolysis reaction center increases the hydrolysis rate by 2 orders of magnitude, but spacing this tertiary amine farther from the reaction center dramatically decreases the reaction rate to the point that there is no increase in rate over the control. Through computational analysis of the reaction pathway, we find that this trend in reaction rate with amine spacing is due to the strength of the intramolecular hydrogen-bonded ring formed in the transition state of the addition of water to the iminium ion. Thus, we expect that other hydrogen bond donors and acceptors can similarly coordinate with water to increase the reaction rate.

We also show the importance of using MP-TST based on the low-energy conformers of a system when calculating reaction kinetics for molecules with a large amount of conformational freedom and several noncovalent bonds accessible in select conformations. As polymer solvolysis is increasingly studied in plastics recycling, we expect to see more computational studies for similar systems and emphasize that MP-TST with highly accurate conformer searching is crucial.

Two main directions for future computational work could further improve the utility of simulations in understanding PDK depolymerization: (1) including more explicit water molecules in the model and (2) including longer polymer chains in the model. First, as we understand that hydrogen bonding plays a large role in the depolymerization of PDKs, it is important to understand how the hydrogen bond network of water will affect intramolecular hydrogen bonding. Second, we identified in this work that the strain in the cross-linker dictates the free energy barrier for DKE hydrolysis. In a networked polymer, the conformational freedom of the cross-linker will be hindered by the network, and we must therefore understand how that hindrance will affect the hydrogen bonding and thus the depolymerization rate.

Finally, learning from the effect of the cross-linker in PDKs, we emphasize that future efforts toward circular polymers for diverse applications should consider the importance of noncovalent effects far from the solvolysis reaction center when designing the system chemistry.

ASSOCIATED CONTENT

Data Availability Statement

Computed data used in the final rate calculations are available on Figshare (json).

Supporting Information

The Supporting Information is available free of charge at https://pubs.acs.org/doi/10.1021/jacs.3c00772.

Detailed computational methods, tables of computational data, permanent DOIs for the computational data available on Figshare, experimental materials, experimental instrumentation, detailed experimental methods, ^{1}H NMR, ^{13}C NMR, and FT-IR of diketoenamines **1**−**5**, and ^{1}H NMR of pristine and chemically recycled C_2 and C_3 triamine polydiketoenamines (PDF)

AUTHOR INFORMATION

Corresponding Authors

Brett A. Helms − *Chemical Sciences Division, The Molecular Foundry, and Materials Sciences Division, Lawrence Berkeley National Laboratory, Berkeley, California 94720, United States;* orcid.org/0000-0003-3925-4174; Email: bahelms@lbl.gov

Kristin A. Persson − *Materials Sciences and Engineering, University of California, Berkeley, Berkeley, California 94720, United States; The Molecular Foundry, Lawrence Berkeley National Laboratory, Berkeley, California 94720, United States;* orcid.org/0000-0003-2495-5509; Email: kapersson@lbl.gov

Authors

Alexander R. Epstein − *Materials Sciences and Engineering, University of California, Berkeley, Berkeley, California 94720, United States;* orcid.org/0000-0002-9914-2388

Jeremy Demarteau − *The Molecular Foundry, Lawrence Berkeley National Laboratory, Berkeley, California 94720, United States;* orcid.org/0000-0002-0311-3575

Complete contact information is available at: https://pubs.acs.org/10.1021/jacs.3c00772

Notes

The authors declare the following competing financial interest(s): B.A.H. is an inventor on the U.S. provisional patent application 62/587,148 and B.A.H., A.E.P., J.D., and K.A.P. are inventors on U.S. provisional patent application 63/390,962, both submitted by Lawrence Berkeley National Laboratory that covers PDKs, as well as aspects of their use and recovery. B.A.H. has a financial interest in Cyklos Materials. The other authors declare that they have no other competing interests.

ACKNOWLEDGMENTS

The authors thank Evan Walter Clark Spotte-Smith for useful discussions on simulations of reaction kinetics.

REFERENCES

(1) Geyer, R.; Jambeck, J. R.; Law, K. L. Production, use, and fate of all plastics ever made. *Science Advances* **2017**, *3*, No. e1700782.

(2) Christensen, P. R.; Scheuermann, A. M.; Loeffler, K. E.; Helms, B. A. Closed-loop recycling of plastics enabled by dynamic covalent diketoenamine bonds. *Nature Chemistry* **2019**, *11*, 442−448.

(3) Saito, K.; Eisenreich, F.; Türel, T.; Tomović, Ž. Closed-Loop Recycling of Poly (Imine-Carbonate) Derived from Plastic Waste and Bio-based Resources. *Angew. Chem., Int. Ed.* **2022**, *61*, No. e202211806.

(4) Gama, N.; Godinho, B.; Marques, G.; Silva, R.; Barros-Timmons, A.; Ferreira, A. Recycling of polyurethane scraps via acidolysis. *Chemical Engineering Journal* **2020**, *395*, 125102.

(5) Häußler, M.; Eck, M.; Rothauer, D.; Mecking, S. Closed-loop recycling of polyethylene-like materials. *Nature* **2021**, *590*, 423−427.

(6) Simón, D.; de Lucas, A.; Rodríguez, J. F.; Borreguero, A. M. Flexible polyurethane foams synthesized employing recovered polyols from glycolysis: Physical and structural properties. *J. Appl. Polym. Sci.* **2017**, *134*, 45087.

(7) Molero, C.; de Lucas, A.; Rodríguez, J. F. Recovery of polyols from flexible polyurethane foam by "split-phase" glycolysis with new catalysts. *Polym. Degrad. Stab.* **2006**, *91*, 894−901.

(8) Vanbergen, T.; Verlent, I.; De Geeter, J.; Haelterman, B.; Claes, L.; De Vos, D. Recycling of Flexible Polyurethane Foam by Split-Phase Alcoholysis: Identification of Additives and Alcoholyzing Agents to Reach Higher Efficiencies. *ChemSusChem* **2020**, *13*, 3835−3843.
(9) Zhu, J.-B.; Watson, E. M.; Tang, J.; Chen, E. Y.-X. A synthetic polymer system with repeatable chemical recyclability. *Science* **2018**, *360*, 398−403.
(10) Cederholm, L.; Wohlert, J.; Olsén, P.; Hakkarainen, M.; Odelius, K. Like Recycles Like": Selective Ring-Closing Depolymerization of Poly (L-Lactic Acid) to L-Lactide. *Angew. Chem., Int. Ed.* **2022**, *61*, No. e202204531.
(11) Abel, B. A.; Snyder, R. L.; Coates, G. W. Chemically recyclable thermoplastics from reversible-deactivation polymerization of cyclic acetals. *Science* **2021**, *373*, 783−789.
(12) Rapagnani, R. M.; Dunscomb, R. J.; Fresh, A. A.; Tonks, I. A. Tunable and recyclable polyesters from CO2 and butadiene. *Nature Chemistry* **2022**, *14*, 877−883.
(13) Mihut, C.; Captain, D. K.; Gadala-Maria, F.; Amiridis, M. D. Review: Recycling of nylon from carpet waste. *Polym. Eng. Sci.* **2001**, *41*, 1457−1470.
(14) Helms, B. A. Polydiketoenamines for a Circular Plastics Economy. *Acc. Chem. Res.* **2022**, *55*, 2753−2765.
(15) Demarteau, J.; Epstein, A. R.; Christensen, P. R.; Abubekerov, M.; Wang, H.; Teat, S. J.; Seguin, T. J.; Chan, C. W.; Scown, C. D.; Russell, T. P.; Keasling, J. D.; Persson, K. A.; Helms, B. A. Circularity in mixed-plastic chemical recycling enabled by variable rates of polydiketoenamine hydrolysis. *Science Advances* **2022**, *8*, eabp8823.
(16) Møller, K. H.; Otkjær, R. V.; Hyttinen, N.; Kurtén, T.; Kjaergaard, H. G. Cost-Effective Implementation of Multiconformer Transition State Theory for Peroxy Radical Hydrogen Shift Reactions. *The Journal of Physical Chemistry A* **2016**, *120*, 10072−10087.
(17) Zheng, J.; Truhlar, D. G. Multi-path variational transition state theory for chemical reaction rates of complex polyatomic species: ethanol + OH reactions. *Faraday Discussions* **2012**, *157*, 59−88.
(18) Viegas, L. P. Simplified Protocol for the Calculation of Multiconformer Transition State Theory Rate Constants Applied to Tropospheric OH-Initiated Oxidation Reactions. *The Journal of Physical Chemistry A* **2021**, *125*, 4499−4512.
(19) Bickelhaupt, F. M.; Houk, K. N. Analyzing Reaction Rates with the Distortion/Interaction-Activation Strain Model. *Angew. Chem., Int. Ed.* **2017**, *56*, 10070−10086.
(20) Bao, J. L.; Truhlar, D. G. Variational transition state theory: theoretical framework and recent developments. *Chemical Society Reviews* **2017**, *46*, 7548−7596.
(21) Epstein, A. R.; Spotte-Smith, E. W. C.; Venetos, M. C.; Andriuc, O.; Persson, K. A. Assessing the Accuracy of Density Functional Approximations for Predicting Hydrolysis Reaction Kinetics. *ChemRxiv* **2023**, DOI: 10.26434/chemrxiv-2023-c8h70 (accessed Mar 13, 2023).
(22) Frisch, M. J.; et al. *Gaussian 16 Revision C.01*; Gaussian Inc.: Wallingford, CT, 2016.
(23) Marenich, A. V.; Cramer, C. J.; Truhlar, D. G. Universal solvation model based on solute electron density and on a continuum model of the solvent defined by the bulk dielectric constant and atomic surface tensions. *J. Phys. Chem. B* **2009**, *113*, 6378.
(24) Chai, J.-D.; Head-Gordon, M. Long-range corrected hybrid density functionals with damped atom−atom dispersion corrections. *Phys. Chem. Chem. Phys.* **2008**, *10*, 6615−6620.
(25) Pracht, P.; Bohle, F.; Grimme, S. Automated exploration of the low-energy chemical space with fast quantum chemical methods. *Phys. Chem. Chem. Phys.* **2020**, *22*, 7169−7192.
(26) Epifanovsky, E.; et al. Software for the frontiers of quantum chemistry: An overview of developments in the Q-Chem 5 package. *J. Chem. Phys.* **2021**, *155*, 084801.
(27) Rappoport, D.; Furche, F. Property-optimized Gaussian basis sets for molecular response calculations. *J. Chem. Phys.* **2010**, *133*, 134105.
(28) Weigend, F.; Ahlrichs, R. Balanced basis sets of split valence, triple zeta valence and quadruple zeta valence quality for H to Rn: Design and assessment of accuracy. *Phys. Chem. Chem. Phys.* **2005**, *7*, 3297−3305.
(29) Rosen, A. QuAcc − The Quantum Accelerator; https://arosen93.github.io/quacc/.
(30) Mathew, K.; et al. Atomate: A high-level interface to generate, execute, and analyze computational materials science workflows. *Comput. Mater. Sci.* **2017**, *139*, 140−152.
(31) Grimme, S. Supramolecular Binding Thermodynamics by Dispersion-Corrected Density Functional Theory. *Chem.—Eur. J.* **2012**, *18*, 9955−9964.

https://doi.org/10.1021/jacs.3c00772
J. Am. Chem. Soc. XXXX, XXX, XXX−XXX